Amorphous Carbon Encapsulation of Metal Aerosol Nanoparticles for Improved Collection and Prevention of Oxidation

William J. Scharmach
Praxair, Inc., 175 E Park Dr. Tonawanda, NY 14150

Munish K. Sharma and Raymond D. Buchner
Dept. of Chemical and Biological Engineering, University at Buffalo (SUNY), Buffalo, NY 14260

Vasilis Papavassiliou
Praxair, Inc., 175 E Park Dr. Tonawanda, NY 14150

Gaurav N. Vajani and Mark T. Swihart
Dept. of Chemical and Biological Engineering, University at Buffalo (SUNY), Buffalo, NY 14260

DOI 10.1002/aic.14218
Published online September 18, 2013 in Wiley Online Library (wileyonlinelibrary.com)

A technique to encapsulate silver nanoparticles in an amorphous carbon matrix to facilitate nanoparticle collection and limit nanoparticle oxidation is presented. A carbon source added to the metal salt precursor solution decomposes to generate amorphous carbon, which forms large aggregates that are efficiently collected by filtration. The carbon matrix can be removed by oxidation with hydrogen peroxide without damaging the silver nanoparticles within it. X-ray diffraction showed no evidence of oxidation of encapsulated particles over a two-week period, whereas bare particles showed oxidation after 1 day. Slight oxidation was observed following carbon removal, but no further oxidation was detected over a subsequent two-week period. Carbon encapsulation improves nanoparticle collection efficiency, relative to direct collection of unagglomerated silver nanoparticles with membrane filters. The yield of metal nanoparticles is increased by a factor 1.5 to 3 using this approach. The encapsulating carbon itself forms dendritic nanostructures that may also be of interest. © 2013 American Institute of Chemical Engineers *AIChE J*, 59: 4116–4123, 2013
Keywords: aerosols, materials, nanotechology

Introduction

Aerosol based nanoparticle production methods present challenges to many common particle collection techniques. A goal of many aerosol-based nanoparticle production processes is to generate minimally agglomerated particles in the size range from 5 to 50 nm.[1] Efficient collection of particles in this size range can prove challenging, especially for the production of metal nanoparticles that are susceptible to oxidation under atmospheric conditions. Collection generally requires expensive equipment such as a modified electrostatic precipitator,[2] baghouse filters with specialized media,[3] or thermophoretic deposition devices.[4] The challenge in direct filtration of ultrafine nanoparticles from a gas stream is selecting a filter that is capable of maintaining collection efficiency without suffering subsequent blockage, pressure drop, or penetration of nanoparticles into the filter, such that they cannot be removed.[5]

The technique presented here is used in conjunction with the flame-based high-temperature reducing jet aerosol reactor developed by Scharmach et al. shown schematically in Figure 1.[6] Carbon coated nanoparticles have been previously reported by several groups, but in contrast to this contribution, the carbon coating in those cases was not intended to encapsulate multiple particles or improve particle collection and handling. Luechinger et al. synthesized copper nanoparticles using a bottom up approach with *in situ* formation of protective shells of graphene to produce air-stable and chemically inert material.[7] Waser et al. synthesized $LiFePO_4$ nanoparticles with a carbon shell via a scalable flame aerosol reactor.[8] Rossier et al. synthesized graphene-coated cobalt nanoparticles via reducing flame synthesis for acid stable nanomagnets.[9] Ernst et al. synthesized carbon coated platinum clusters for catalytic applications using a scalable single-step flame spray pyrolysis reactor.[10] Kammler et al. synthesized carbon coated titania particles using a continuous one step flame synthesis method.[11]

The HTRJ reactor system uses hydrogen reduction to produce metal, rather than metal oxide, nanoparticles in the presence of water vapor. Hot combustion products pass through a nozzle to produce a high-temperature reducing jet. An injected precursor solution is rapidly atomized, evaporated, and

Correspondence concerning this article should be addressed to M. T. Swihart at swihart@buffalo.edu.

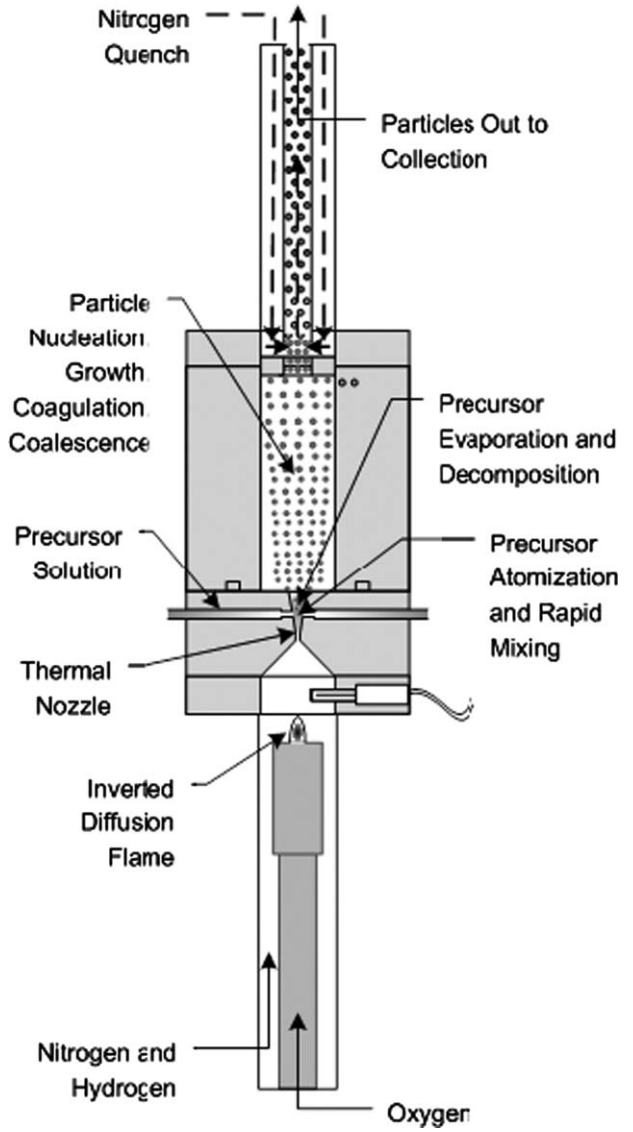

Figure 1. Schematic diagram of the high-temperature reducing jet (HTRJ) reactor.

decomposed in the high-temperature expanding jet, initiating particle formation. Particles are then quenched and collected downstream via filtration. The ability to vary the composition of the precursor solution injected into the reactor not only provides control of the particle composition, but also provides an opportunity for deposition of surface coatings on the produced particles. When an excess of a low-enthalpy carbon source, such as ethanol or acetic acid, is introduced with the precursor, microparticles of an amorphous carbon matrix, each encapsulating multiple metal nanoparticles, are formed. This encapsulation provides protection from oxidation and produces agglomerates of large overall size that are relatively easy to collect by filtration and to recover from the filter media in high yield. The carbon coating can subsequently be removed in solution.

Experimental

Amorphous carbon coating using high-temperature reducing jet synthesis

The prototype high-temperature reducing jet reactor system (Figure 1) has been described in detail previously.[6] It consists of a burner in which a relatively small flow of oxygen (~2 SLM) and a larger flow of hydrogen and nitrogen (~12 SLM total) support an inverted diffusion flame (oxidant on the inside, fuel on the outside) at the tip of the oxygen inlet lance. The flame temperature is controlled by varying the oxygen flow while always using excess hydrogen. This provides a hydrogen-rich, oxygen-free environment in the postcombustion region. The hot combustion products are accelerated through a converging-diverging nozzle. The precursor is delivered within the nozzle. Downstream of the nozzle, the precursors evaporate and decompose and particles nucleate. At the exit of the reactor (after a residence time of ~50 ms) a substantial (>100 SLM) quench flow of nitrogen is added to arrest particle growth and sintering.

Precursors used in these experiments included silver nitrate (ACS reagent, ≥99.0% silver nitrate, Acros Organics) and acetic acid (ACS reagent grade glacial acetic acid 100% assay, J.T. Baker). The silver nanoparticles described here were synthesized with metal precursor concentrations of 10 mM, with and without acetic acid addition, in order to determine the yield of collected and recovered particles. The reactor was operated for a total of 2 h for each experiment, which consumed approximately 360 mL of precursor solution. Encapsulated nanoparticles were produced with 10 vol % acetic acid in the aqueous precursor solution. Nanoparticles were collected using a 293 mm dia. PVDF membrane filter with 0.2 micron pore size (Millipore, Durapore brand). These filters provide efficient particle collection with minimal pressure drop at the total gas flow rates (>100 SLM including the quench gas flow) used here. Collected particles were dried *in situ* at the end of a synthesis run by flowing water/precursor-free gas through the sample. Particles were removed from the filter paper using sonication in acetone. The resulting particle dispersion was centrifuged to remove acetone as a supernatant. The carbon-coated particles were then treated with 3 vol % hydrogen peroxide in a beaker to remove carbon encapsulation. Contact of the particles with peroxide resulted in immediate production of gas bubbles. To speed up the etching process, beaker contents were heated gently, but were not allowed to boil. After 2 days of etching, the nanoparticles were washed with milli-Q water and centrifuged for 10 min at 10,000 rpm (ca. 10,000 G) and redispersed for further characterization. The extended etching time was used to ensure that all amorphous carbon was removed. The mass of the particles was determined at three points (1) amorphous carbon coated silver nanoparticles on the filter paper, (2) acetone washed carbon-encapsulated particles from the filter paper, and (3) particles after amorphous carbon removal by treatment with hydrogen peroxide solution. The yield was compared with the yield of silver nanoparticles produced without carbon encapsulation. Samples were dried overnight using a vacuum desiccator before weighing. The reported results are the average value of three independent batches for each condition. Thermogravimetric analysis using a NETZSCH TG209 F1 model was used to determine the silver content of the carbon-encapsulated samples by comparing the mass loss from carbon-encapsulated particles to that from bare particles upon heating. All TGA Samples were heated from ambient temperature to 1000°C under nitrogen at a heating rate of 10°C/min.

Nanoparticle Characterization

The silver nanoparticles were analyzed by a series of methods: X-ray diffraction (XRD) (Rigaku Ultima IV X-Ray

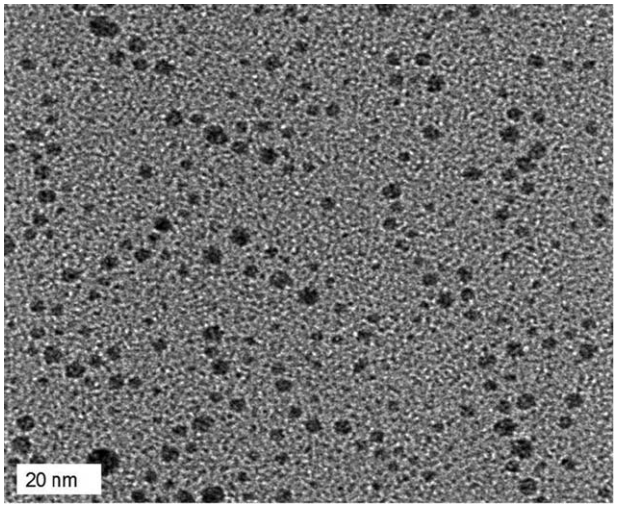

Figure 2. Low-magnification transmission electron micrograph of silver nanoparticles produced without carbon encapsulation and collected directly onto a TEM grid via electrostatic precipitation.

The majority of the particles are below 10 nm in dia.

Diffractometer), transmission electron microscopy (TEM) (JEOL JEM 2010 at an accelerating voltage of 200KV), and scanning electron microscopy (AURIGA™ CrossBeam® Workstation (FIB-SEM) from Carl Zeiss SMT). A custom-built electrostatic sampler, similar to that described by Dixkens and Fissan,[12] was used for collecting particles directly onto TEM grids for offline analysis. Fourier transform infrared spectroscopy (FTIR, VERTEX 70 Spectrometer, Bruker Corp.), UV–visible absorption spectroscopy (ThermoElectron Corp., Spectronic Genesys 6), and high-pressure liquid chromatography (Agilent 1260 Infinity Isocratic LC system) were used to characterize the particles and the molecules adsorbed to their surface or created during amorphous carbon removal. A custom-made confocal Raman microspectrometer based on an inverted Nikon TE200 microscope equipped with a He-Ne (Coherent, 632.8 nm) excitation laser, fiber-input MS3501i imaging monochromator/spectrograph (Solar TII), and Hamamtsu S9974 series CCD cooled to −60°C was used to acquire Raman spectra of the particles after amorphous carbon removal.

Results and Discussion

In the experiments described here, we produced silver nanoparticles from silver nitrate in water, and amorphous carbon encapsulated silver nanoparticles from silver nitrate in 10 vol % aqueous acetic acid. Silver nitrate is used here as a prototypical metal precursor which decomposes thermally at temperatures below 500°C, to produce silver or silver oxide and gaseous byproducts (NO_2 and NO). Silver nitrate is a low-cost silver salt that is highly soluble in water (ca. 2.16 kg per L), which melts at 212°C and decomposes at about 440°C to yield silver oxides and nitrous oxides.[13] Thus, upon rapid heating of silver nitrate, we expect evaporation of water from precursor droplets, leaving solid $Ag(NO_3)_2$ particles that then melt and evaporate or sublime and decompose. This might lead to formation of Ag_2O particles directly from $Ag(NO_3)$, or to nucleation of Ag or Ag_2O from the gas phase.[14] In the presence of excess hydrogen, any oxides produced (Ag_2O) will be reduced to metallic silver. The silver particles produced, with or without carbon encapsulation, are generally less than 10 nanometers in diameter. Typical nonagglomerated silver particles produced without acetic acid are shown in Figure 2.

Acetic acid, added as a carbon source, is a low-cost acid that boils at 118°C and decomposes at about 440°C[15] to produce carbomethene,[16] water, methane and hydrogen.[16,17] Unimolecular decomposition of acetic acid is known to occur by the following parallel reactions

$$H_3CCOOH \rightarrow CH_4 + CO_2$$

$$H_3CCOOH \rightarrow H_2CCO + H_2O$$

The majority of the decomposition products are carbon dioxide and methane,[18] whose production is thermodynamically more favorable than carbomethene and water.[19] However, kinetically, both pathways are competitive. Both methane and carbon dioxide could serve as carbon sources for deposition of carbonaceous material on the silver particles. However, the thermal decomposition of methane requires a high process temperature, even in the presence of a catalyst,[17] and the excess hydrogen in the system would tend to shift the reaction toward methane.[20] A more likely route is the conversion of carbon dioxide and hydrogen to carbon monoxide and water via the following reaction (reverse water gas shift)

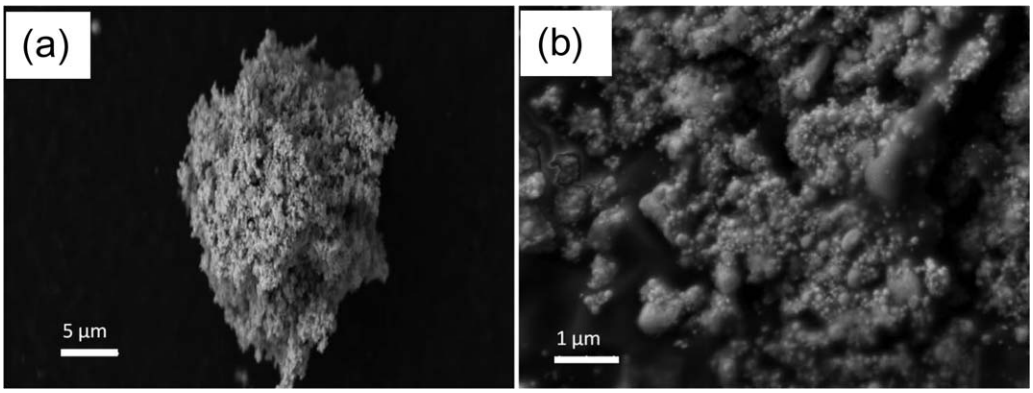

Figure 3. Scanning electron micrographs of silver nanoparticles encapsulated in amorphous carbon.

Image (a) shows an agglomerate measuring ~27 μm long. Image (b) is a magnified version of image (a), showing many silver nanoparticles visible within the aggregate.

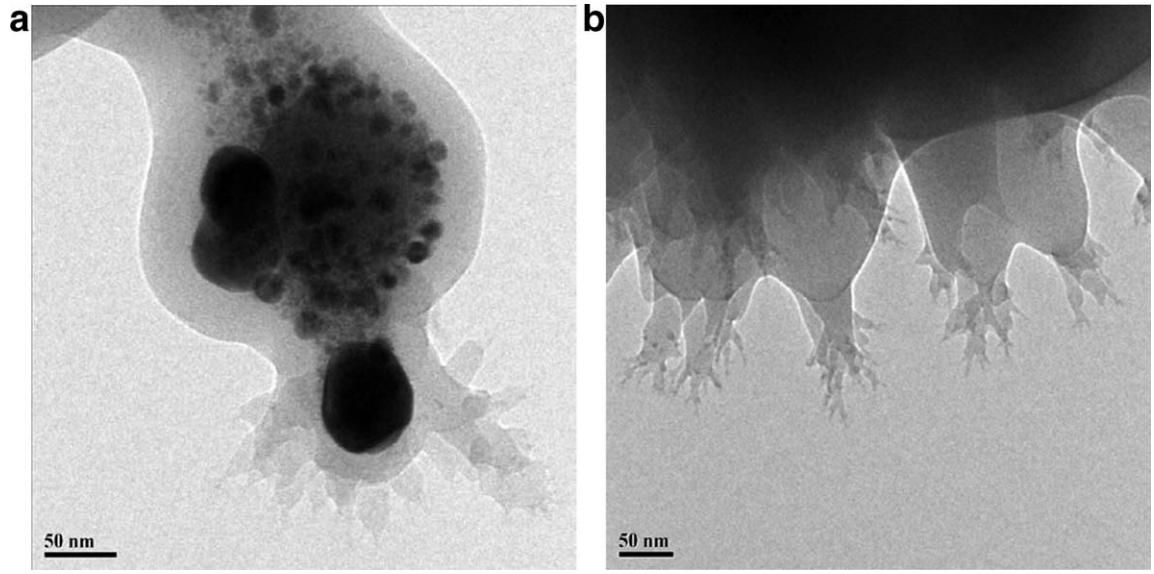

Figure 4. High-magnification transmission electron micrographs of amorphous carbon encapsulated silver nanoparticles showing the dendritic morphology of the carbon.

These show (a) many silver nanoparticles encapsulated in an amorphous carbon shell, and (b) dendritic morphology of the encapsulating carbon nanostructures.

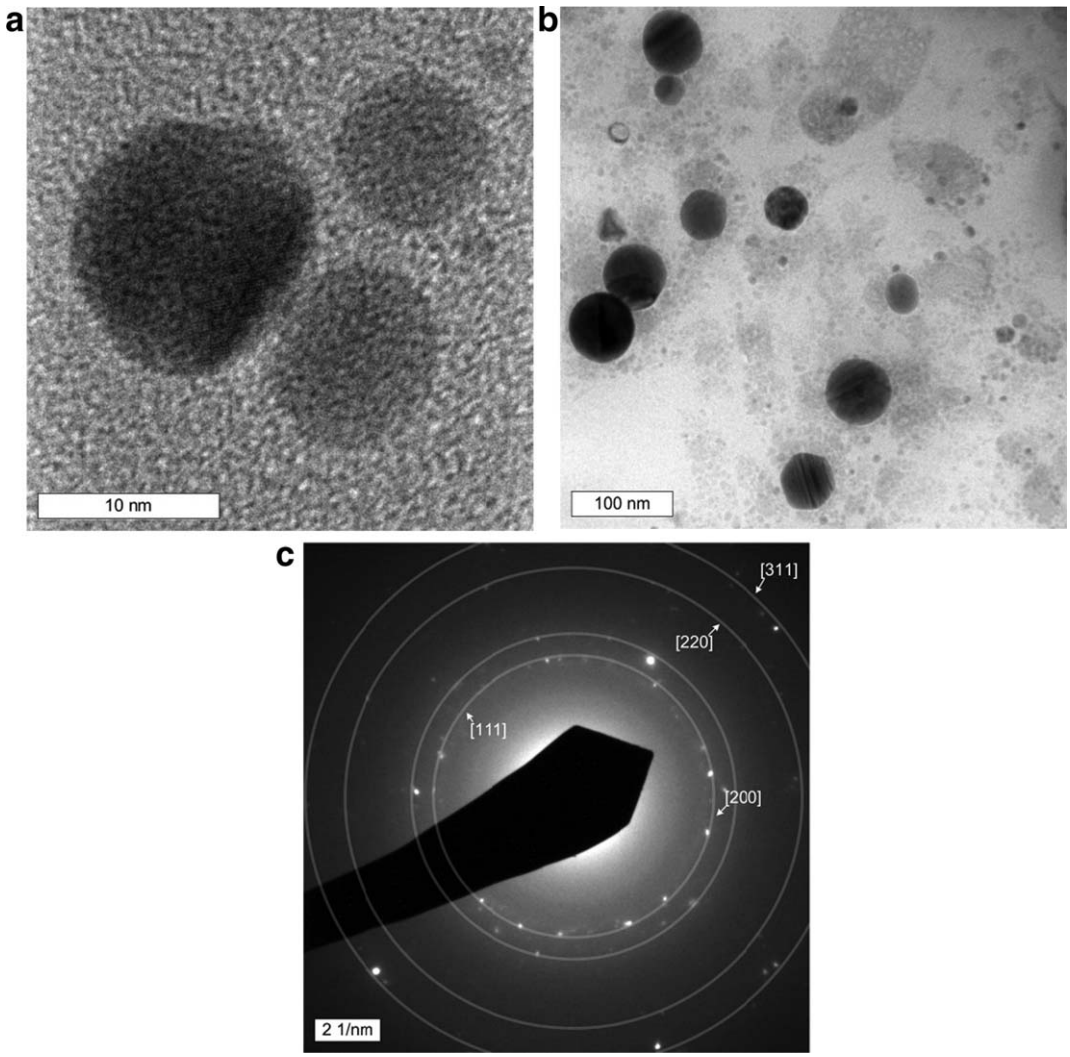

Figure 5. Transmission electron micrographs (a, b) of amorphous carbon encapsulated silver, and (c) selected area electron diffraction pattern of carbon encapsulated silver.

Table 1. Yields of Silver Nanoparticles and Carbon-Coated Silver Nanoparticles

Process condition	Yield (Ave. ± St. Dev.)[a]
Bare silver nanoparticles on filter paper (no carbon)	17.0±1.2
Carbon encapsulated silver nanoparticles on filter paper (total mass, including carbon)	63.5±8.3
Carbon encapsulated silver nanoparticles recovered from filter paper (total mass, including carbon)	53.8±10.4
Silver content of encapsulated silver nanoparticles on filter paper (based upon thermogravimetric analysis)	52.7±8.3
Silver content of encapsulated silver nanoparticles recovered from filter paper (based upon thermogravimetric analysis)	44.7±10.4
Silver particles recovered after carbon removal	25.3±1.5

[a]Yield is the mass of material (including carbon for encapsulated particles) divided by the mass of silver supplied in the precursor solution. Three independent experiments were performed for each condition. Too few bare particles could be removed from the filter paper to obtain a reliable measurement.

$$CO_2 + H_2 \leftrightarrow CO + H_2O$$

The formation of a carbonaceous coating could then occur via the Boudouard reaction

$$2CO \leftrightarrow C + CO_2$$

This reaction is exothermic and is favorable at the moderately high temperatures prevailing in the reactor. Similar results have been seen from uncatalyzed water gas shift reactions done in quartz tubes.[21] The role of the nanoparticles in the formation of the carbonaceous layer is not fully understood, but silver nanoparticles have catalytic properties,[22,23] which may enhance the formation of carbon.[22,24]

Figure 3 shows scanning electron microscope (SEM) images of particles produced in this system from silver nitrate in 10% acetic acid. Particles are entirely encased in large carbonaceous deposits, preventing general oxidation of particles. Figure 4 shows high-resolution transmission electron micrographs (TEM) of amorphous carbon encapsulated silver nanoparticles. Figure 4a shows many silver nanoparticles encapsulated in an amorphous carbon shell, and Figure 4b shows the dendritic morphology of the encapsulating carbon nanostructures. Figure 5 shows TEM images of silver nanoparticles directly sampled onto a TEM grid using electrostatic deposition. Figure 5 shows particles encapsulated in a carbonaceous layer, along with the corresponding selected area electron diffraction (SAED) pattern. Particles in Figure 5 were collected from a sample stream that had been diluted with nitrogen. The majority of silver particles (by number) are below 10 nm in diameter, but there is a small fraction of larger particles of about 50 nm dia., similar to the other experiments using silver nitrate. Figure 5a shows a transmission electron microscopy image of the carbon encapsulated silver particles. The coating is not apparent in this view due to the similarity of the amorphous coating with the carbon support film on the TEM grid. A lower magnification image is shown in Figure 5b. The lattice fringes in the high-resolution images have a spacing of 2.37 Å, matching the expected 2.36 Å spacing of fcc silver (111) planes. Likewise, the SAED ring diameters in Figure 5c are consistent with metallic silver.

Table 1 summarizes the effect of carbon encapsulation on the yield of silver nanoparticles from the process. The average yield of bare silver particles collected on the filter without carbon encapsulation was 17%. Only a small fraction of this could be effectively removed from the filter membrane upon which the particles were collected. For carbon

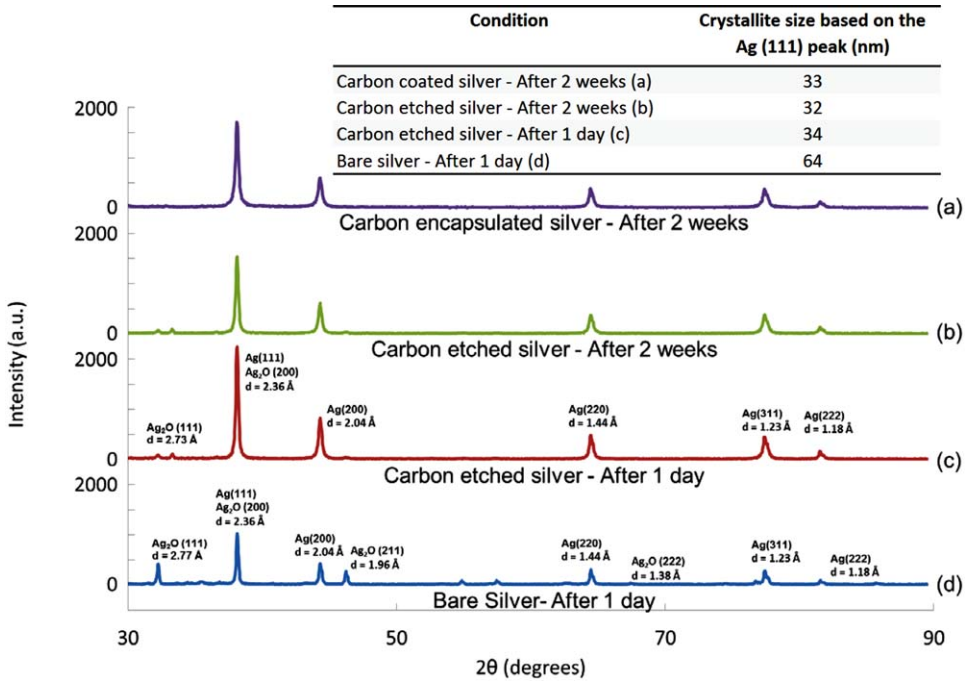

Figure 6. Powder X-Ray diffraction patterns of (a–c) carbon encapsulated silver particles (a) after 2 weeks of storage time under light and air (b) 2 weeks after carbon removal, and (c) 1 day after carbon removal, and (d) uncoated silver particles (produced without using a carbon source) after 1 day under light and air.

[Color figure can be viewed in the online issue, which is available at wileyonlinelibrary.com.]

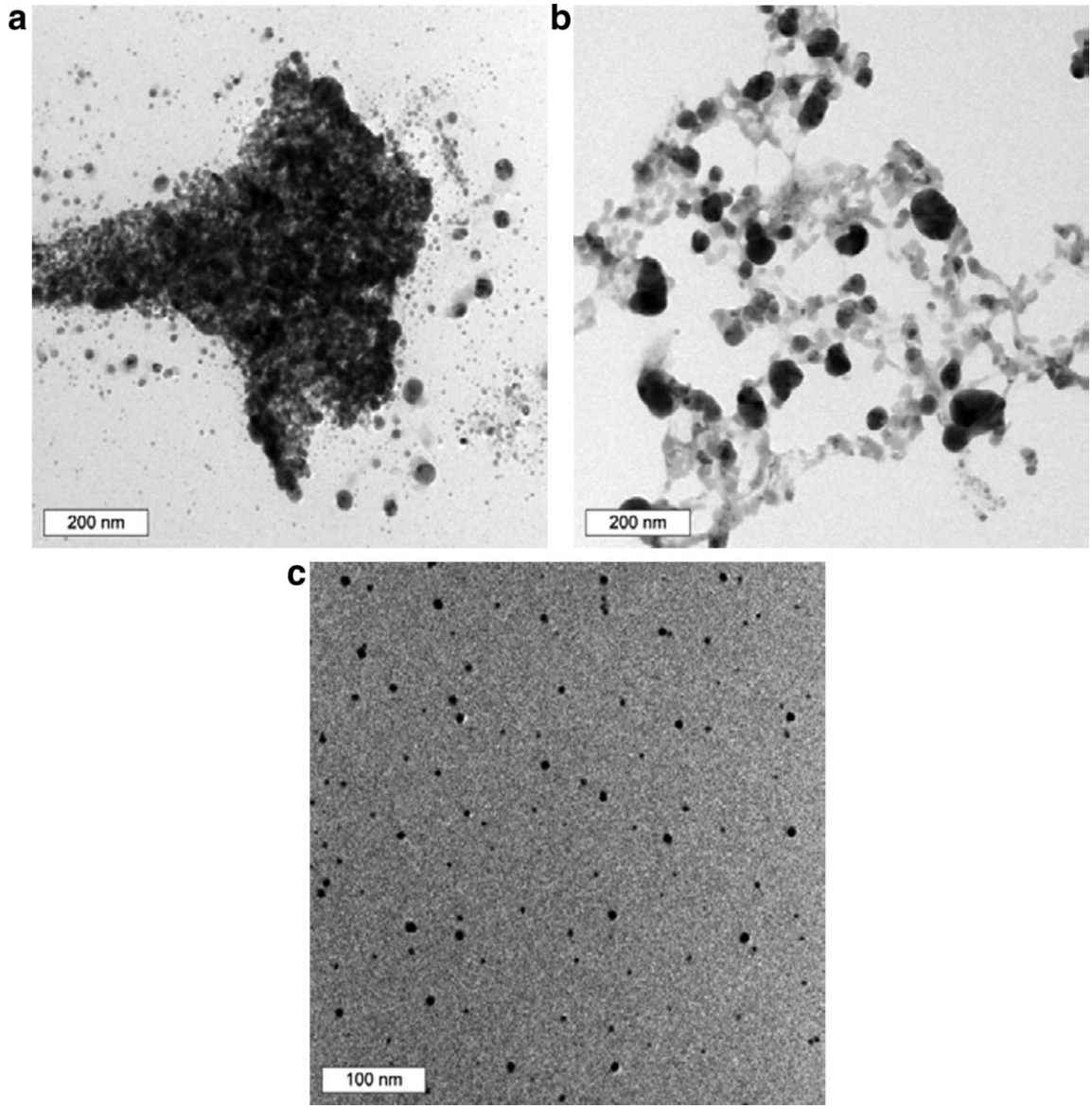

Figure 7. Representative transmission electron micrographs at varying extents of carbon removal by 3 vol % H_2O_2.

Image (a) shows carbon encapsulated particles (b) carbon encapsulated particles after ~2 h in 3 vol % H_2O_2, and (c) carbon encapsulated particles after overnight exposure to 3 vol % H_2O_2.

encapsulated particles, nearly 4 times as much mass was collected on the filter membrane, compared to bare particles. The mass of silver plus carbon collected was about 63.5% of the mass of silver supplied to the system. Most of this mass was successfully removed from the filter via sonication in acetone. Even after carbon removal by hydrogen peroxide treatment, the mass of free particles collected was about 1.5 times the mass of bare silver particles collected on the filter. All of these yields would be expected to increase with process scale. Losses by diffusion are important for these small nanoparticles, and will diminish substantially with increasing process scale (larger conduits for flow with shorter residence times at higher gas flow rates yield reduced diffusion losses).

A better estimate of the potential yield of silver may be given by results of thermogravimetric analysis. The silver content of the carbon-coated particles removed from the filter paper can be estimated by comparing the mass loss from them, upon heating to a temperature that pyrolyzes the carbon, to the mass loss from the bare silver nanoparticles. Upon heating to 1000°C, carbon-encapsulated nanoparticles lost about 18% of their mass, whereas pure silver particles lost about 7% of their mass, and silver particles from which the carbon encapsulation had been removed lost about 5% of their mass. This suggests that the carbon content of the encapsulated particles is between 11 and 18%, and probably near 13%. Assuming that the silver content of the encapsulated particles removed from the filter paper is 82%, gives a yield of silver in the encapsulated particles recovered on the filter paper of 52.1% of the silver supplied to the reactor. Similarly, the yield of silver in the encapsulated particles removed from the filter paper is 44.1%. Thus, we estimate that about three times as much silver is collected on the filter for experiments using carbon encapsulation compared to experiments without carbon encapsulation.

Furthermore, in order to test the effectiveness of the encapsulation as a coating capable of protecting the silver from oxidation, particles were exposed to the ambient atmosphere and examined 2 weeks later with the carbon matrix

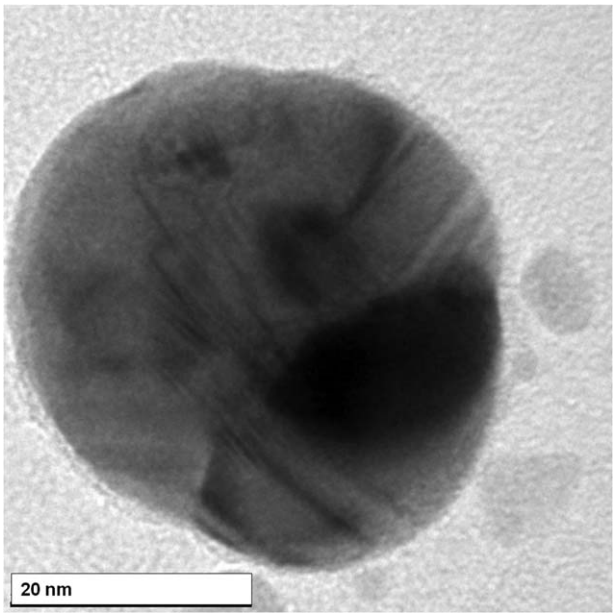

Figure 8. TEM image of a relatively large silver particle after amorphous carbon removal, showing a thin residual coating on its surface.

still intact (without H_2O_2 treatment), and finally with the matrix removed (etched) and compared against pure silver powder without any carbon encapsulation exposed to ambient conditions for 1 day. Figure 6 shows a comparison of four XRD patterns. Figure 6 compares powder X-ray diffraction (XRD) patterns from carbon-encapsulated silver particles after 2 weeks of storage (Figure 6a), after carbon removal and storage for 1 day (Figure 6c) and 2 weeks (Figure 6b), and pure silver nanoparticles stored for 1 day (Figure 6d). The appearance of XRD peaks corresponding to crystalline Ag_2O (cubic) confirms slight oxidation of silver in air 1 day after carbon removal. However, the relative intensity of oxide peaks did not increase further over a two week period, suggesting that further oxidation did not occur. Figure 6d shows evidence of silver oxide formation with formation of Ag_2O (111) peak at 32.24° with a d-spacing of 2.77 Å and Ag_2O (211) peak at 46.23° with a d-spacing of 1.96 Å. Smaller peaks likely arise from AgO or other silver oxide phases. The crystallite size of the Ag (111) peak calculated using the Scherrer equation was found to be 32 ± 2 nm in Figure 6a–c), which were all for the same sample after different treatments. No peak broadening was observed after carbon removal, suggesting that etching with 3% hydrogen peroxide does not affect crystallite size of the nanoparticles. This suggests that the loss of material during the carbon encapsulation process does not result from oxidation and dissolution of silver during the peroxide treatment, but simply from incomplete collection by centrifugation and losses during washing steps. Such handling-related losses should diminish at increased scale. The crystallite size from the partially oxidized bare Ag particles was estimated from the Scherrer equation to be 64 nm. The larger crystallite size for bare Ag particles may reflect inhibition of silver particle aggregation and sintering by the carbon encapsulation, such that smaller particles are obtained when a carbon source is added, however, we have not explored this effect in detail. The crystallite size determination by XRD could also be influenced by selective oxidation of smaller particles or by overlap of the Ag(111) peak with the smaller Ag_2O(200) peak in this sample.

The amorphous carbon coating can be removed using hydrogen peroxide or other oxidizing agents. Base piranha solution, a strong oxidizer made up of ammonium hydroxide and hydrogen peroxide, has also been successfully tested for carbon removal. Both agents provide an effective and easily implemented method of readily removing amorphous carbonaceous material originating from the preparation procedure.[25,26] Figure 7 shows three TEM images, of samples for which the particles were reacted with 3 vol % hydrogen peroxide successively longer reaction times, roughly 2 h for Figure 7b and overnight for Figure 7c, resulting in varying degrees of removal of the amorphous carbon. Here, we can see the decomposition of the carbonaceous layer until the silver particles are free from encapsulation.

XRD before (Figure 6a,b,c) and after amorphous carbonaceous coating removal, indicate that the silver has not oxidized during the peroxide treatment. This stability, as well as the long-term stability in air described above, may result from a graphene or graphitic layer that forms during the production of nanoparticles. Such a layer is visible in the TEM image shown in Figure 8. That particle is much larger than average, and, therefore, has lower curvature and a longer electron-beam path through the particle periphery. This provides enough contrast to visually distinguish the thin coating from the background. We also carried out Raman spectroscopy of the carbon layer on the surface of the particle after the amorphous carbon layer has been removed. The large peak exhibited by the carbon layer near 1473 cm^{-1} is similar to the $A_g(2)$ pentagonal pinch mode[27] measured in fullerenic carbon nanostructures.[17,20,27,28] Carboxylic acid groups on the outside of the particles following hydrogen peroxide treatment act as a dispersing agent, stabilizing the nanoparticles in water. A Fourier transform infrared spectrum of the particles after treatment with hydrogen peroxide is shown in Figure 9, indicating the presence of carbonyl, hydroxyl, and carboxyl functional groups.

During the coating removal, the amorphous carbonaceous layer is oxidized, leading to the formation of hydroxyl groups, carboxylic acid and carboxylate groups and a small amount of aldehydes and ketones on the surface of the particle.[29,30] These functional groups aid in temporarily

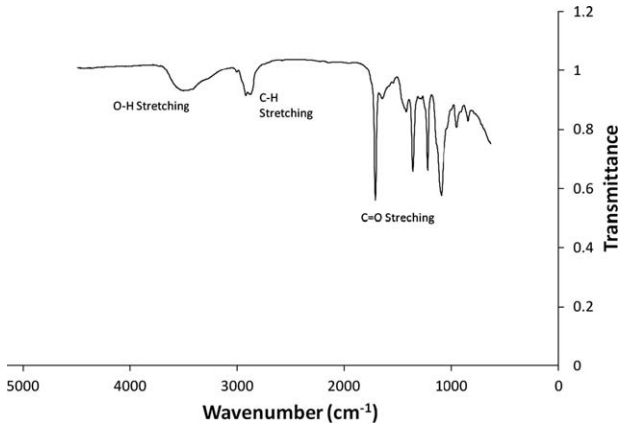

Figure 9. The FTIR spectrum of silver nanoparticles after treatment with hydrogen peroxide shows the presence of —OH and —C═O functional groups.

dispersing nanoparticles in water. Excess carbon in the sample is oxidized to carbon monoxide and/or carbon dioxide and leaves the solution as a gas. The thin residual layer of functionalized carbon that appears to remain on the silver surface serves to stabilize particles until it is replaced with a suitable capping agent for producing stable, high-concentration dispersions.

Conclusion

We have demonstrated amorphous carbon encapsulation of metal nanoparticles produced in a flame-based high-temperature reducing jet aerosol reactor system. This carbon encapsulation approach can be a valuable method of improving particle collection in aerosol-based nanoparticle synthesis systems and protecting metal particles from atmospheric oxidation during subsequent storage and handling. This was achieved with acetic acid added to the aqueous metal salt precursor solution as a carbon source. The result is an efficient way to boost collection efficiency and enable the use of lower cost collection techniques. Hydrogen peroxide was used to remove the amorphous carbon matrix. X-ray diffraction showed no evidence of oxidation of encapsulated particles over a two-week period, whereas bare particles showed oxidation after 1 day. Slight oxidation was observed following removal of the encapsulating carbon, but no further oxidation was detected by XRD over a two-week period following carbon removal. The removal of the amorphous carbon matrix left a thin graphitic carbon coating decorated with carboxylic acid groups on the surface of the silver, which aided in temporarily dispersing the silver nanoparticles. This approach can potentially be used with many different types of metal nanoparticles synthesized in aerosol processes under reducing conditions.

Acknowledgments

This work was partially supported by The National Science Foundation (CBET-0652042), and the University at Buffalo Integrated Nanostructured Systems Instrumentation Facility.

Literature Cited

1. Swihart MT. Vapor-phase synthesis of nanoparticles. *Curr Opin Colloid Interface Sci*. 2003;8(1):127–133.
2. Kim W, Jung JH, Song DK, Kim H, Kim YJ, Kim SS. Effect of temperature on carbon nanoparticle collection efficiency using photoelectric ESP. *Sci Total Environ*. 2009;407(6):2136–2141.
3. Mueller R, Mädler L, Pratsinis SE. Nanoparticle synthesis at high production rates by flame spray pyrolysis. *Chem Eng Sci*. 2003; 58(10):1969–1976.
4. Gonzalez D, Nasibulin AG, Baklanov AM, et al. A new thermophoretic precipitator for collection of nanometer-sized aerosol particles. *Aerosol Sci. Technol*. 2005;39(11):1064–1071.
5. Hinds WC. *Aerosol Technology: Properties, Behavior, and Measurement of Airborne Particles*. 2nd ed. New York: Wiley; 1999.
6. Scharmach WJ, Buchner RD, Papavassiliou V, Pacouloute P, Swihart MT. A high-temperature reducing jet reactor for flame-based metal nanoparticle production. *Aerosol Sci Technol*. 2010;44(12): 1083–1088.
7. Luechinger NA, Athanassiou EK, Stark WJ. Graphene-stabilized copper nanoparticles as an air-stable substitute for silver and gold in low-cost ink-jet printable electronics. *Nanotechnology*. 2008;19(44): 6.
8. Waser O, Buechel R, Hintennach A, Novak P, Pratsinis SE. Continuous flame aerosol synthesis of carbon-coated nano-$LiFePO_4$ for Li-ion batteries. *J Aerosol Sci*. 2011;42(10):657–667.
9. Rossier M, Koehler FM, Athanassiou EK et al. Energy-efficient noble metal recovery by the use of acid-stable nanomagnets. *Ind Eng Chem Res*. 2010;49(19):9355–9362.
10. Ernst FO, Buchel R, Strobel R, Pratsinis SE. One-step flame-synthesis of carbon-embedded and -supported platinum clusters. *Chem Mater*. 2008;20(6):2117–2123.
11. Kammler HK, Pratsinis SE. Carbon-coated titania nanostructured particles: Continuous, one-step flame-synthesis. *J Mater Res*. 2003; 18(11):2670–2676.
12. Dixkens J, Fissan H. Development of an electrostatic precipitator for off-line particle analysis. *Aerosol Sci Technol*. 1999;30(5):438 – 453.
13. Patnaik P. *Handbook of Inorganic Chemicals*. New York: McGraw-Hill; 2003.
14. Wang R-C, Gao Y-S, Chen S-J. Simple synthesis and size-dependent surface-enhanced Raman scattering of Ag nanostructures on TiO_2 by thermal decomposition of silver nitrate at low temperature. *Nanotechnology*. 2009;20(37):375605.
15. Logvinenko V, Polunina O, Mikhailov Y, Mikhailov K, Bokhonov B. Study of thermal decomposition of silver acetate. *J Therm Anal Calorim*. 2007;90(3):813–816.
16. Mackie JC, Doolan KR. High-temperature kinetics of thermal decomposition of acetic acid and its products. *Int J Chem Kin*. 1984; 16(5):525–541.
17. Cantelo RC. The thermal decomposition of methane. *J Phys Chem*. 1924;28:1036–1048.
18. Kirshenbaum AD, Streng AG, Hauptschein M. The thermal decomposition of silver salts of perfluoro carboxylic acids. *J Am Chem. Soc*. 1953;75:3141–3145.
19. Nguyen MT, Sengupta D, Raspoet G, Vanquickenborne LG. Theoretical study of the thermal decomposition of acetic acid: decarboxylation versus dehydration. *J Phys Chem*. 1995;99(31):11883–11888.
20. Cantelo RC. Thermal decomposition of methane. *II. J Phys Chem*. 1926;30:899–901.
21. Bustamante F, Enick RM, Killmeyer RP, et al. Uncatalyzed and wall-catalyzed forward water-gas shift reaction kinetics. *AIChE J*. 2005;51(5):1440–1454.
22. Li W-X, Stampfl C, Scheffler M. Insights into the function of silver as an oxidation catalyst by ab initio atomistic thermodynamics. *Phys Rev B*. 2003;68(16):165412/165411-165412/165415.
23. Zhao Z, Carpenter MA. Support-free bimodal distribution of plasmonically active ag/agox nanoparticle catalysts: attributes and plasmon enhanced surface chemistry. *J Phys Chem C*. 2013;117(21): 11124–11132.
24. Bechoux K, Marie O, Daturi M et al. Infrared evidence of room temperature dissociative adsorption of carbon monoxide over Ag/Al2O3. *Catalysis Today*. 2012;197(1):155–161.
25. Choi W-K, Park S-G, Takahashi H, Cho T-H. Purification of carbon nanofibers with hydrogen peroxide. *Synth Met*. 2003;139(1):39–42.
26. Suzuki T, Suhama K, Zhao X, Inoue S, Nishikawa N, Ando Y. Purification of single-wall carbon nanotubes produced by arc plasma jet method. *Diamond Relat Mater*. 2009;16(4-7):1116–1120.
27. Lenski DRF, M. S. Raman and optical characterization of multilayer turbostratic graphene grown via chemical vapor deposition. *J Appl Phys*. 2011;110.
28. Ferrari AC, Meyer JC, Scardaci V, et al. Raman spectrum of graphene and graphene layers. *Phys Rev Lett*. 2006;97(18):187401.
29. Rakov E. Chemistry of Carbon Nanotubes. *Nanomaterials Handbook*. Boca Raton, FL: CRC Press; 2006.
30. Gómez-Serrano V, Acedo-Ramos M, López-Peinado AJ, Valenzuela-Calahorro C. Oxidation of activated carbon by hydrogen peroxide. *Study of surface functional groups by FT-i.r. Fuel*. 1994;73(3):387–395.

Manuscript received Nov. 13, 2012, and revision received July 31, 2013.